1 **Two-dimensional monitoring of air pollution in Madrid using a MAXDOAS-2D**

2 **instrument**

3

4 David Garcia-Nieto[1, 2], Nuria Benavent[1, 2], Rafael Borge[2] and Alfonso Saiz-Lopez[1]

5

6 [1] Department of Atmospheric Chemistry and Climate, Institute of Physical Chemistry

7 Rocasolano, CSIC, Madrid 28006, Spain

8 [2] Universidad Politécnica de Madrid, UPM, 28006 Madrid, Spain

9

10 *Corresponding author: Alfonso Saiz-Lopez (a.saiz@csic.es)

11

12 **Abstract**

13

14   Trace gases play a key role in the chemistry of urban atmospheres. Therefore,

15 knowledge about their spatial distribution is needed to fully characterize air quality in

16 urban areas. Using a new Multi-AXis Differential Optical Absorption Spectroscopy

17 (MAXDOAS)-2D instrument, along with an inversion algorithm (bePRO), we report the

18 first two-dimensional maps of nitrogen dioxide (NO_2) and nitrous acid (HONO)

19 concentrations in the city of Madrid, Spain. Measurements were made during two

20 months (May 6 –July 5 2019) and peak mixing ratios of 12 ppbv and 0.7 ppbv for NO_2

21 and HONO, respectively, were observed in the early morning in the southern part of

22 the downtown area. We found good general agreement between the MAXDOAS-2D

23 mesoscale observations -which provide a typical spatial range of a few kilometers- and

24 the in-situ measurements provided by Madrid´s air quality monitoring stations. In

25 addition to vertical profiles, we studied the horizontal gradients of NO_2 in the surface

layer by applying the different horizontal light path lengths in the two spectral regions included in the NO_2 spectral analysis: ultraviolet (UV, at 360 nm) and visible (VIS, 477 nm). We also investigate the sensitivity of the instrument to infer vertically-distributed information on aerosol extinction coefficients and discuss possible future ways to improve the retrievals. The retrieval of two-dimensional distributions of trace gas concentrations reported here provides valuable spatial information for the study of air quality in the city of Madrid.

1 Introduction

Air pollution in urban areas has become a concern in our society because it represents a major risk to human health and the environment (WHO, 2019). Air quality is often expressed as the state of air pollution in terms of gaseous pollutant concentrations as well as size and number of particulate matter that may affect human health, ecosystems and climate (Monks et al., 2009). Integral understanding of air pollution requires knowledge about the sources, pollutants, chemical composition and spatial distribution, and their transport phenomena in the atmosphere (EEA, 2019).

Madrid, Spain, has suffered from severe air pollution in recent years, with episodes of large nitrogen dioxide (NO_2) and ozone (O_3) concentrations. In an effort to control and reduce high pollution events, the local government has enforced some traffic restriction measures (Izquierdo et al., 2020) and has set up several in-situ air quality monitoring stations over the city's metropolitan area. These in-situ instruments -as of today- cannot measure some important trace gases present in the atmosphere and their values are only representative of the immediate surrounding of the instruments and at surface level. There is therefore a need for mesoscale analysis (both in horizontal and vertical, in the order of 10 km) of urban air pollution that could

complement the in-situ measurements. With this aim, we have deployed a Multi AXis Differential Optical Absorption Spectroscopy (MAXDOAS) instrument for air pollution measurements in Madrid. MAXDOAS is a widely used technique for the detection of trace gases in the atmosphere and it is based on the wavelength dependent absorption of scattered sunlight by atmospheric constituents (Platt and Stutz, 2008). In addition to routinely monitored species such as NO_2 and O_3, MAXDOAS provides mesoscale measurements of other trace gases that are relevant to understand atmospheric chemistry, such as nitrous acid (HONO), formaldehyde (HCHO) or glyoxal (CHOCHO). Over the past few years, we have reported trace gas measurements in Madrid using the MAXDOAS technique (Wang et al., 2016; Garcia-Nieto et al., 2018; Benavent et al., 2019) as well as pollutants trend analysis and chemical transport modelling (Borge et al., 2018; Cuevas et al., 2014; Saiz-Lopez et al., 2017).

For this work, a new two-dimensional MAXDOAS instrument (which will be described in Sect. 3 and will be hereafter referred to as MAXDOAS-2D) has been built, tested and set up to take continuous measurements in Madrid. This instrument represents a follow-up development to our previous one-dimensional instrument (MAXDOAS-1D, see Wang et al., 2016) that incorporates the capability of moving in the azimuthal dimension, therefore allowing the collection of spectra pointing at any angular direction. This additional capability allows the measurement of both the horizontal and vertical trace gas (e.g. NO_2) distribution throughout the city and in turn the generation of two-dimensional maps of trace gas concentrations. Several works using two-dimensional MAXDOAS instruments have been carried out in recent years (e.g. Ortega et al., 2015, Yang et al., 2019, Schreier et al., 2020, Dimitropolou et al., 2020). These studies were mostly focused on mapping the NO_2 distribution in urban environments and assessing its role for air quality monitoring.

3

80   Here we present two months of MAXDOAS-2D measurements of scattered

81   sunlight spectra. The measurements were taken from May 6, 2019 to July 5, 2019, with

82   focus on the evaluation of NO_2 vertical concentration profiles and the characterization

83   of horizontal light path lengths. We also provide the retrieval of HONO as an example

84   of the potential of the MAXDOAS-2D to provide spatial information also on other trace

85   gases relevant to urban atmospheric chemistry. An assessment of the relation

86   between the MAXDOAS data and the in-situ measurements of NO_2 in the city was

87   carried out. Sect. 2 provides details of the DOAS technique while Sect. 3 describes the

88   experimental setup. The inversion methods and the atmospheric parameters chosen

89   for the analysis are detailed in Sect. 4. The two-dimensional NO_2 and HONO

90   distributions, an evaluation of the light path geometries, along with their relative

91   probabilities, and an assessment of horizontal mixing ratio gradients near the surface

92   are discussed in Sect. 5.

93

94   **2 Brief introduction to the DOAS method**

95

96   The DOAS basic idea is described by the Beer-Lambert law, which models the

97   exponential attenuation of spectral irradiance when it traverses a certain sample that

98   contains some absorbers:

99

100
$$I(\lambda, L) = I_0(\lambda)\, exp\left(-\sum_i \int_0^L \sigma_i(\lambda)\, \rho_i(s)ds\right) \qquad (1)$$

101

102   where λ is wavelength, σ_i and ρ_i stand for -respectively- the absorption cross section

103   and concentration of a given absorber i along the path, while the pair I_0 and I

104   represent the spectral irradiances at the beginning and end of the process at study.

105 The absorption processes are integrated over the photon paths (with infinitesimal

106 path ds) and summed over every present absorber (Platt and Stutz, 2008).

107

108 Specifically, the MAXDOAS technique is based on the study of the differential

109 spectral absorption structures that are produced in the measured scattered sunlight

110 spectra (Hönninger et al., 2004; Plane and Saiz-Lopez, 2006; Platt and Stutz, 2008). The

111 main principle is based on identifying the narrowband absorption features within the

112 measured optical density taking out the broadband optical density, mainly generated

113 by Rayleigh and Mie scattering, as well as by instrumental effects. On the other hand,

114 an analogous process is done on the trace gases absorption cross sections by means

115 of filtering out the broadband spectral features, hence producing the so-called

116 differential absorption cross sections, which are unique for each trace gas, acting as

117 their "fingerprints" and therefore enabling their specific detection.

118

119 For MAXDOAS, I_0 stands for the solar spectrum (known as the Fraunhofer

120 spectrum, with no Earth atmospheric absorptions), while I represents the recorded

121 ground-based spectrum, which includes all the absorption and scattering processes.

122 However, and since the actual photon path is difficult to determine with accuracy (see

123 Sect. 4), the MAXDOAS calculations are done using relative absorptions between two

124 different optical paths: a zenith spectrum -that contains less absorptions and is

125 assumed as a reference spectrum- and other spectrum pointing to a given elevation

126 angle. Therefore, the direct product of the method is the differential slant column

127 density (DSCD), which can be defined as the difference in the integrated concentration

128 of a given absorber between the two selected pointing directions (more details about

129 the numerical procedure that lies behind can be found in Honninger et al., 2004, Plane

130 and Saiz-Lopez, 2006 and Platt and Stutz, 2008). Finally, these DSCDs are used as the

131 main input for the profile retrieval algorithms, which simulate the state of the

132 atmosphere with the purpose of reproducing the measured DSCDs. This final step

133 yields the optimal vertical concentration profiles.

134

135 **3 Experimental**

136

137   Briefly, MAXDOAS-1D instruments consist of a light collector attached to a

138 stepper motor that scans the atmosphere at different Viewing Elevation Angles (VEA,

139 see Fig. 1). The main feature added to the MAXDOAS-2D instrument is an additional

140 stepper motor for the azimuthal movement, hence allowing the light collector to freely

141 point to any angular direction in the atmosphere. This allows the evaluation of trace

142 gases absorptions for different Viewing Azimuth Angles (VAAs) (Fig. 1).

143

144 **3.1 MAXDOAS-2D description**

145

146   A MAXDOAS-2D instrument (Fig. 2) was built by the Atmospheric Chemistry and

147 Climate group at the Institute of Physical Chemistry Rocasolano (IQFRCSIC). Its main

148 elements are based on our previous MAXDOAS-1D instrument: a light collector

149 attached to a stepper motor, along with a focusing lens (80 mm focal length) are

150 responsible for collecting the scattered sunlight. An Ocean Optics, SMA 905 optical

151 fiber of 1-meter length conducts the light through an Ocean Optics, HR4000

152 spectrometer (which incorporates a linear silicon CCD array as detector). The

153 spectrometer wavelength ranges roughly from 300 nm to 500 nm and offers an

154 estimated spectral resolution (full width at half maximum) of about 0.5 nm. An

155 additional stepper motor was included for azimuthal movement. The instrument

156 incorporates all its components in an outdoor unit. Therefore, to maintain the

157 spectrometer temperature as steady as possible -for both mechanical and wavelength

158 calibration purposes- a Peltier cell was included. Additionally, an UPS device provides

159 the power supply and eliminates possible strong power peaks. Two webcams take

160 pictures of the cloud cover at each VAA, and monitor the instrument itself. The

161 instrument is autonomous and it runs on a homemade Java software. This software

162 controls the movement, the spectra collection and recording, the surrounding

163 accessories and automatically keeps it continuously measuring as long as the Sun is
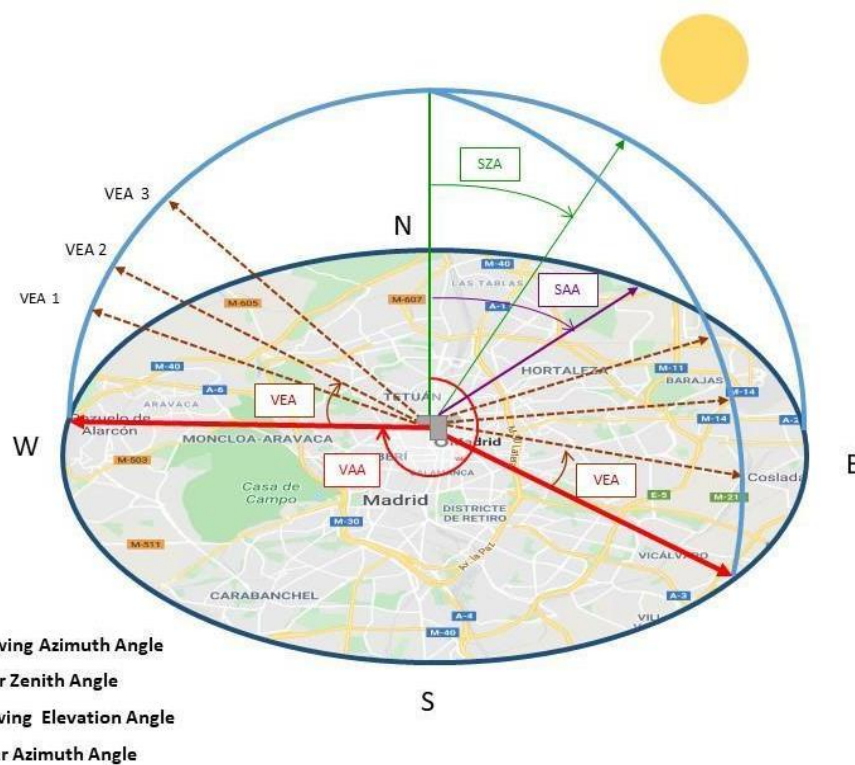
164 over the horizon.

165

166

167 **Figure 1**. MAXDOAS-2D geometry diagram, the background of this picture represents

168 the Madrid city center taken from Google Maps.

169

170 **3.2 Location**

171

The MAXDOAS-2D instrument is located at the main campus of the Spanish National Research Council (CSIC) in Madrid, Spain. It is placed on the roof of the Instituto de Ciencias Agrarias (ICA) at a latitude of 40.4419° N and a longitude of 3.6875° W. The height of the building is approximately 70 m above ground level. This location in downtown Madrid can be classified as an urban site, with the usual weather of continental areas at mid-latitudes (i.e. hot and dry summers and cold winters), with prevalence of clear sky days during the year. NO_2 typically presents strong spatial concentration gradients in urban areas and traffic hot-spots have been reported in Madrid (Borge et al., 2016). This makes it difficult to clearly predict how NO_2 will be distributed, i.e., there is not a clear azimuthal direction preference for higher NO_2 at a certain time. However, mesoscale simulations suggest that higher NO_2 mixing ratios can be expected in the southern part of Madrid, considering population distribution and commuting patterns (Picornell et al., 2019).

Due to some obstacles that blocked a clear view in some of the VAAs, a small aluminum tower was built to overcome the viewing obstacles and the MAXDOAS-2D instrument was fixed on top of it (see Fig. 2). Once the instrument was set up, we aligned it for both angular movements -azimuthal and zenithal- with respect to the geographical north and the local horizontal (i.e. perpendicular to the gravitational plumb), respectively. This process was performed in two steps: first, the light collector was coarsely oriented using levels and a compass. Then, the alignment was refined doing a vertical scan of the Sun (which has a very well-known position vector) and its angular surroundings at several different times of a clear sky day. The angular differences between the measurements and the center of intensity of the registered spectra (a similar approach was done in Ortega et al., 2015) were estimated and the associated correction applied to the instrument.
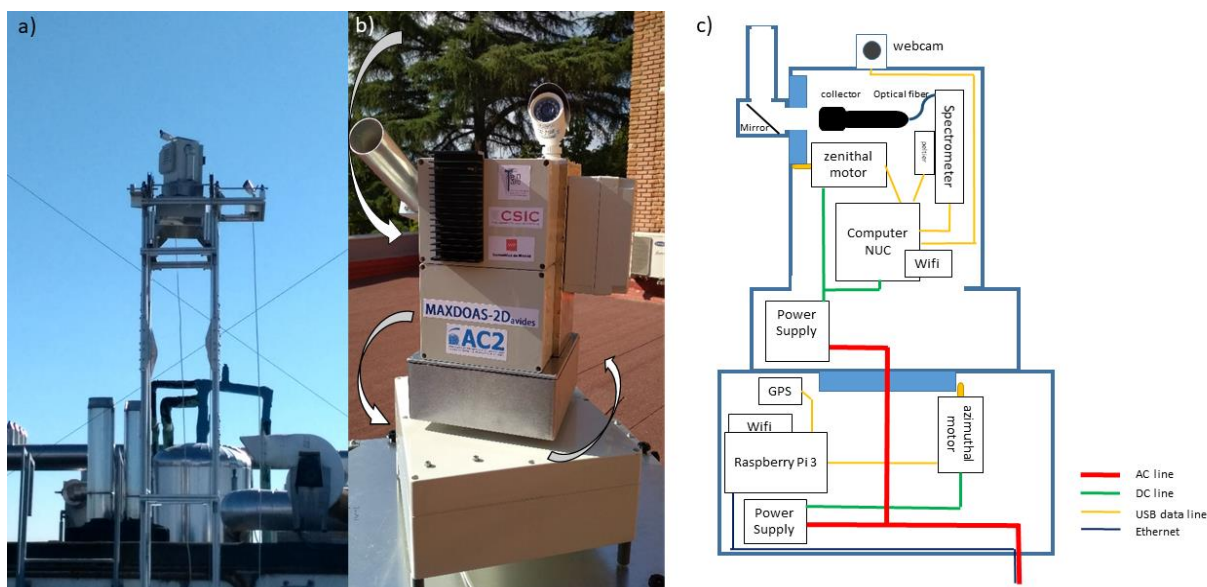
199

Figure 2. a) Aluminum tower with the instrument installed on top of it; b) MAXDOAS-2D instrument; c) MAXDOAS-2D scheme.

3.3 Measurements set up

In order to sample and analyze a representative portion of the atmosphere over Madrid, selected angular directions were chosen. Starting at a VAA of 0º (pointing to the north), the MAXDOAS-2D rotated clockwise using steps of 20º in azimuth. In each azimuth direction, the ensuing VEA vector was used: 1, 2, 3, 5, 10, 30 and 90 degrees. Therefore, an entire azimuthal lap was completed when the light collector was back again at VAA of 0 degrees.

For every measured spectrum, the spectrometer was able to correct for both electronic offset and dark current effects. Other important parameters for the measurements such as the integration time and the number of scans taken in each angular direction were automatically calculated. More specifically, for this study we set the goal of completing an azimuthal lap in approximately one hour (mainly for an

217   easier interpretation of the results and for the subsequent comparison with in-situ

218   instruments of Madrid´s air quality monitoring network). Hence, we chose 24 seconds

219   as the maximum exposure time in each angular combination.

220

221   The main advantage of this set-up is that we can observe the daily NO_2

222   variability over the entire city with a moderate temporal resolution (1-hour). The main

223   disadvantage is that observations for each VAAs averaged over such a short integration

224   period may be affected by microscale phenomena. Nonetheless, NO_2 concentration

225   gradients are particularly strong in space (Borge et al., 2016). Therefore, this time

226   resolution may be well suited to characterize both the azimuthal and the horizontal

227   gradients of NO_2.

228

229   **4 Analysis methods**

230

231   The absorptions of the molecular oxygen dimer (O_4) and NO_2 were measured

232   for the entire campaign and for two spectral windows: 352-387 nm (UV region) and

233   438-487 nm (VIS region). The analysis settings applied for the UV and VIS regions are

234   summarized in Tables 1 and 2, respectively. These configurations mainly follow those

235   used in Wagner et al., 2019.

236

237   **Table 1.** DOAS spectral settings for the retrieval of O_4 and NO_2 in the UV.

Parameter	Value
Fitting window	352-387 nm

Wavelength calibration	Based on reference solar atlas (Chance and Kurucz, 2010)
Zenith reference	Scan
Polynomial Order	5
Intensity Offset	Order 2
Shift	The measured spectra and Ring were allowed to shift and stretch (order 1) in wavelength.

Molecule	Cross section
O_4	293 K (Thalman and Volkamer, 2013)
NO_2	298 K (Vandaele et al., 1998)
O_3 a	273 K (Serdyuchenko et al., 2014)
O_3 b	223 K (Serdyuchenko et al., 2014)
HCHO	297 K (Meller and Moortgat, 2000)
HONO	296 K (Stutz et al., 2000)
Ring_a	Calculated by QDOAS
Ring_b	Ring_a spectrum multiplied by λ^{-4}

238

239 **Table 2.** DOAS spectral settings for the retrieval of O_4 and NO_2 in the VIS.

Parameter	Value
Fitting window	438-487 nm
Wavelength calibration	Based on reference solar atlas (Chance and Kurucz, 2010)
Zenith reference	Scan
Polynomial order	5
Intensity offset	Order 2
Shift	The measured spectra and Ring were allowed to shift and stretch (order 1) in wavelength.

Molecule	Cross section
O_4	293 K (Thalman and Volkamer, 2013)
NO_2	298 K (Vandaele et al., 1998)
O_3 a	273 K (Serdyuchenko et al., 2014)
O_3 b	223 K (Serdyuchenko et al., 2014)
H_2O	296 K (Rothman et al., 2010)
Glyoxal	296 K (Volkamer et al., 2005)
Ring_a	Calculated by QDOAS

Ring_b   Ring_a spectrum multiplied by λ^{-4}

240 ───

241   The selected differential absorption cross sections -along with the spectral

242   window and parameters included in Tables 1 and 2- were adjusted to the measured

243   differential optical density using the QDOAS spectral fitting software (http://uv-

244   vis.aeronomie.be/software/QDOAS/). Figure 3 shows examples of spectral detection

245   of O_4 and NO_2 for both the UV and VIS regions.

246
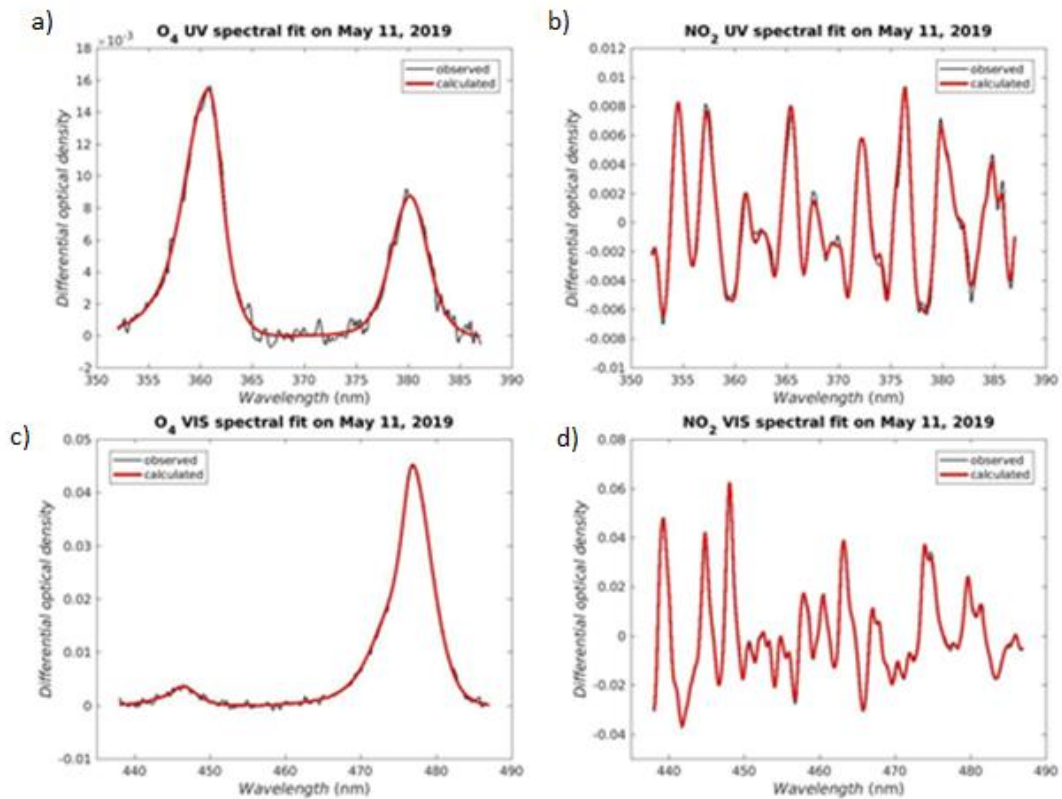
248   **Figure 3**. Spectral detection of O_4 (a) and (c) and NO_2 (b) and (d), red lines represent

249   the calculated optical densities and black lines are the measured optical densities. The

250   viewing geometry of each detection was: (a) VEA 2° and SZA 26.4°; (b) VEA 3° and SZA

251   24.7°; (c) VEA 1° and SZA 22.6° and (d) VEA 1° and SZA 48.7°.

252

4.1 Cloud-screening and quality filtering

The algorithms for MAXDOAS retrievals of trace gas vertical profiles are based on estimating the light paths (along with their corresponding scattering probability). A significant cloud cover could noticeably impact the calculations, mainly because of multiple scattering effects, adding large uncertainties to the retrieval process. For this reason, the set of measured spectra was cloud-screened using the cloud-free AERosol RObotic NETwork (AERONET) database. The AERONET databases are reported with three quality levels, in particular, we used the Level 2.0 (cloud-screened and quality-assured) database provided by the AERONET instrument in Madrid. This information is combined with the photos taken by the camera installed on the MAXDOAS. As mentioned in Sect. 3.1, this webcam points at the same azimuthal direction as the light collector. We estimated the cloud cover using a code that gets the RGB coordinates - the three chromatists of the blue, green and red- and it changes them into LCh coordinates -L indicates lightness, C represents chroma and h is the hue angle. Based on criteria of luminosity, colour and saturation, the code estimates the cloud index (percentage of estimated cloud cover in a given azimuthal sky view). Filtering out cloudy skies with precision is rather challenging, therefore we established a threshold to get as many clear sky views as possible. In order to do that, we first crossed our measured DSCDs with the AERONET 2.0 database, and subsequently, using the photos, we discarded the cycles taken with an estimated cloud index higher than 40 %.

In addition to cloud screening, several other quality filters were applied to the DSCDs: firstly, every DSCD that yielded either a relative uncertainty larger than 1 or a residual root mean square (RMS) higher than 0.01 (in optical density units) was rejected. After that, we estimated the DSCDs detection limit for a given trace gas as the ratio of the residual RMS (in optical density units) associated to each DSCD and the maximum value of the differential cross section of that trace gas. Then, we discarded the DSCDs that had an absolute value lower than twice the derived detection limit (a

14

281 similar approach was carried out in Peters et al., 2012). Finally, we used the daily

282 plus/minus three standard deviation criterion that AERONET applies for its cloud-

283 filtered data, keeping the DSCD that falls within plus/minus three standard deviations

284 from each daily mean.

285

286 **4.2 Inversion algorithm and vertical profiles**

287

288   An inversion algorithm method is applied to the measured DSCDs to estimate

289 the light paths and subsequently derive the trace gas vertical concentration profile.

290 For this work we have used the bePRO inversion algorithm (Clémer et al., 2010). The

291 original calculation was built based on the Optimal Estimation Method (OEM; Rodgers,

292 2000) and it comprises two steps: first, the light paths and the vertical profiles of

293 irradiance extinction are calculated using the O_4 DSCDs; then, the target trace gas

294 vertical concentration profile is retrieved using the corresponding light paths and

295 measured absorption. In order to do that, bePRO simulates the atmospheric state

296 characterizing several different physical phenomena including pressure and

297 temperature vertical profiles, Rayleigh and Mie scattering events (along with their

298 respective phase functions), the effect of the surface albedo, the light path geometries

299 or the irradiance extinction processes. Once the atmospheric vector state is defined,

300 its combination with a certain vertical concentration profile results in the simulated

301 DSCDs. This vertical profile is iterated until the generated set of simulated DSCDs is

302 optimized with respect to the measured DSCDs so that the residual is minimized. As a

303 result, an optimal vertical profile is obtained when the iteration is finished for each

304 MAXDOAS cycle.

305

306   The measured O_4 DSCDs are used to estimate the light paths for each VEA since

307 they are related to the square of the atmospheric O_2 profiles, which are well-known.

308   This profile is fairly steady during the day and does not heavily depend on chemistry

309   factors. Therefore, the measured O_4 DSCDs can provide information on the irradiance

310   extinction in the atmosphere. This extinction profile is usually associated with the

311   aerosol extinction coefficients and thus, its vertical integration yields the aerosol

312   optical depth (AOD). These aerosol extinction profiles are required to subsequently

313   evaluate trace gas profiles since they strongly affect the relative light paths and hence

314   the concentration profiles derived from them.

315

316   Once the light paths are computed, and with the purpose of best simulating the

317   measured DSCDs, a linear analysis process is performed for the measured DSCDs of

318   the target trace gas, yielding the optimal vertical concentration profile. The vertical

319   integration of this concentration profile is called the vertical column density (VCD).

320

321   The retrieval consists of an iterative, nonlinear system of equations, and hence

322   there is no unique solution. This means that an a priori profile is needed, both for

323   starting the iterations and to avoid the final solution to be non-realistic (i.e. with no

324   physical meaning). In order to construct these a priori profiles we used exponentially

325   decreasing curves as follows:

326

327    $$ap\,(z) = \frac{VC_i}{sh} exp\left(\frac{-z}{sh}\right) \tag{2}$$

328

329   where $ap\,(z)$ is the a priori vertical profile at a certain altitude z, VC_i is the

330   vertical integration of the profile for the MAXDOAS cycle *i* and *sh* is the scaling height

331   constant. We used 0.5 km as the scaling height constant for all the a priori profiles

332   (Hendrick et al., 2014). Regarding the VC, we assumed an AOD of 0.05 for the O_4

333   retrieval, while for NO_2 we applied the geometrical approximation followed in

334   Hönninger et al., 2004, taking the measured DSCD at VEA 30° for every MAXDOAS

335 cycle. This approximation assumes that most of the absorption events are located

336 below the scattering height.

337

338   With respect to the remaining atmospheric parameters, we chose typical values

339 for urban environments: surface albedo of 0.07, correlation length of 0.4 km and an a

340 priori covariance factor of 1 (see Hendrick et al., 2014). Concerning the vertical grid of

341 the retrievals, we chose the following layers: from the ground to 8 km height we used

342 layers of 200 m thickness. Then, we divided the remaining height, up to 90 km, in levels

343 of 2 km thickness each. We use the air number density vertical profile since it is directly

344 related to the number of O_4 absorptions, and therefore to the O_4 DSCDs. Hence the

345 relative differences, particularly for lower VEAs, between the measured and simulated

346 O_4 DSCDs are usually assigned to aerosol extinction. Note however, as shown below,

347 that uncertainties in the air number density profiles -arising from uncertainties in the

348 values or shape of the temperature and pressure profiles- could also contribute to such

349 differences (Fig. 4).
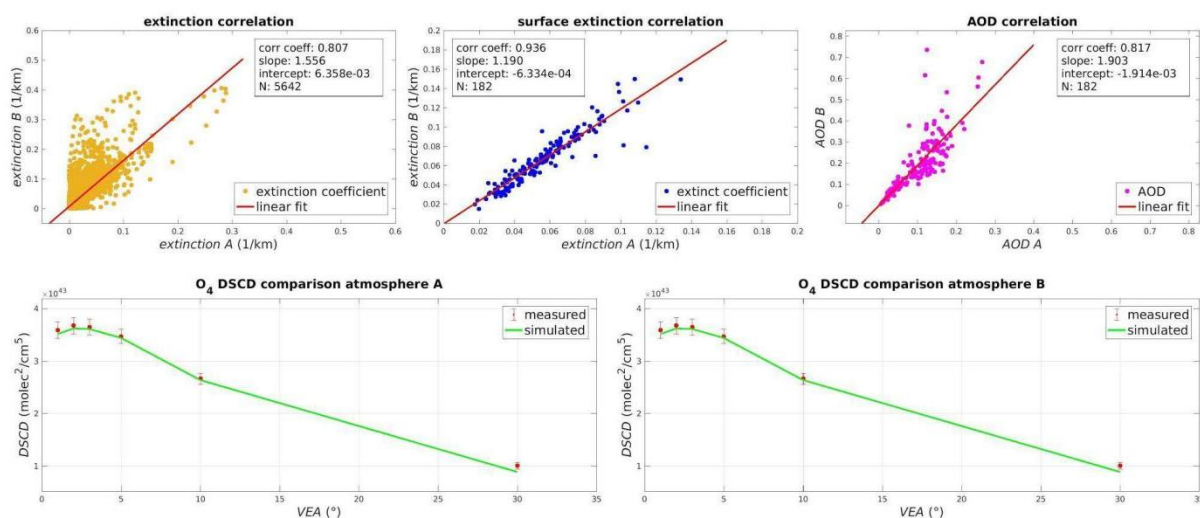
350

351

352 **Figure 4**. Comparison of retrieved aerosols using two different atmospheric

353 profiles: the US Standard (atmosphere A) and the US Standard adapted to the altitude

354   above sea level of Madrid (atmosphere B). The comparison was carried out for a clear

355   sky day (May 11, 2019).

356

357   Here we compare the simulation of O_4 DSCDs using two different sets of

358   atmospheric profiles: i) the US Standard, and ii) the same profile but interpolating the

359   pressure profile to Madrid´s height above sea level (mean value of 667 m). This means

360   that the temperature profile is assumed to be the same but the pressure profile is

361   shifted less than 10%, so there are no major variations within the profiles. The lower

362   row in Fig. 4 shows that both atmospheric profiles result in almost the same set of

363   simulated O_4 DSCDs, however the aerosol extinction coefficients differ significantly

364   (although less for the surface layer coefficients, defined as the extinction coefficients

365   within the ground layer, between 0 and 200 m height), and consequently, the AOD

366   also varies. From this we infer that:

367

368   i)   the retrieval is mainly driven by the measured DSCDs, which leaves a

369   relatively low weight for the chosen atmospheric profiles (pressure and

370   temperature). Therefore, we can obtain consistent correlations between

371   the measured and simulated O_4 DSCDs.

372

373   ii)   we cannot reliably assign the extinction coefficients at each layer to

374   aerosols (especially for atmospheric layers above the surface layer), but

375   rather consider them as irradiance extinction coefficients.

376

377   Furthermore, we have assessed the impact of the pressure and temperature

378   profiles choice on the trace gas retrieval. As can be noted in Fig. 5, there is no

379   significant effect coming from this choice on the simulated NO_2 DSCDs. These are

380 basically the same (and with very good agreement with the measured DSCDs), as well

381 as the derived concentration coefficients and their integration (VCD).
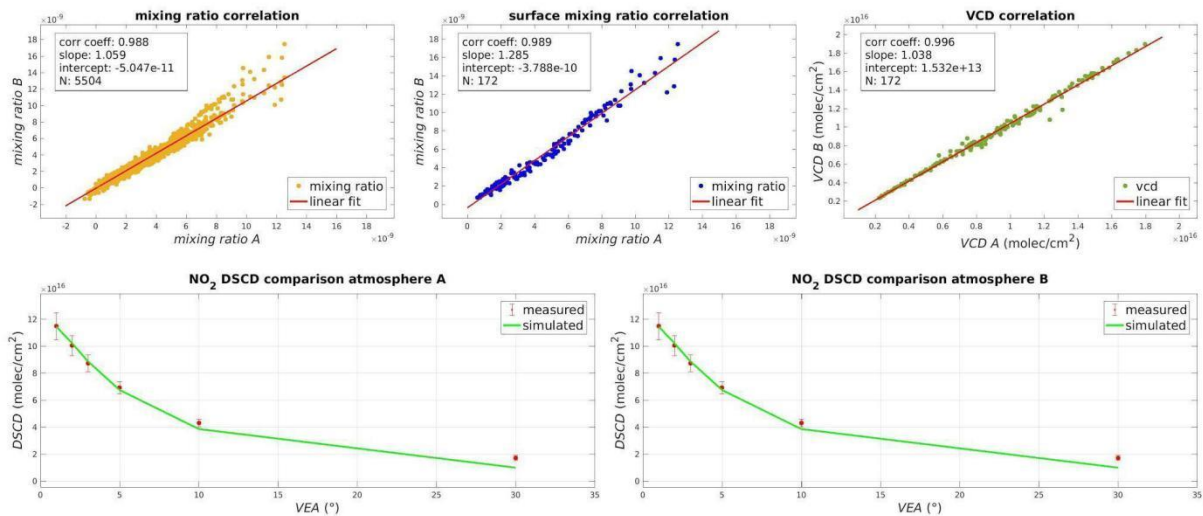
382

383

384 **Figure 5**. NO$_2$ retrieval comparison using two different atmospheric profiles: the US

385 Standard (atmosphere A) and the US Standard adapted to the altitude above sea level

386 of Madrid (atmosphere B). The comparison was carried out for a clear sky day (May

387 11, 2019), considered as representative of the measurement period.

388

389 We further evaluated if a similar behavior can be expected for larger variations

390 in the pressure and temperature profiles. We first obtained the average surface

391 temperature and pressure values during the campaign (May-July, 2019). With the

392 inclusion of these values in the retrieval, we found that, within the first 10 km height,

393 the RMS of the relative variations with respect to the standard atmosphere were about

394 8 %. Although it is a small change, it is indeed not negligible. Nonetheless, when

395 evaluating light paths, the relative changes were below 2%. Therefore, here we use

396 the US Standard atmospheric profiles for the NO$_2$ retrievals.

397

398   Table 3 summarizes the average uncertainties (using one standard deviation for

399   each component) of the retrieval, along with their relative contributions, for the

400   ground layer (0-200 m height). The mean, overall uncertainty for NO_2 in both spectral

401   regions is in the order of 10%.

402

403   **Table 3.** Summary of average uncertainties of the retrieval in both spectral regions.

Variable \ Trace gas	NO_2 UV (%)	NO_2 VIS (%)
Irradiance Extinction	7.7	5.1
DSCD	4.8	3.2
Surface Mixing Ratio	5.0	8.7
Total	10	11

404

405   **4.3 Estimation of NO_2 horizontal gradients**

406

407   Making use of the different paths that photons travel through the atmosphere

408   for different wavelengths, we can estimate the horizontal distribution of NO_2. We use

409   the estimated horizontal light paths at two wavelengths, 360.8 nm and 477 nm, for

410   the surface layer (0-200 m height). The different light paths at 360.8 and 477 nm

411   provide information about the horizontal distribution of NO_2 mixing ratios within the

412   surface layer. In order to evaluate these horizontal paths, we have a code that

413   implement the RTM equations based on previous pioneering work (Solomon et al.,

414   1987). These equations yield a vector of scattering events along with their respective

415   probabilities. If we take a VEA of 0 degrees (i.e. horizontal viewing), then the scalar

416   product of such vectors produces the length of the horizontal light path.

417

418   We computed this for every MAXDOAS cycle and for both wavelengths, yielding

419 typical -representative- horizontal distances of about 8-10 km for the UV (at 360.8 nm)

420 and between 15-20 km for the VIS window (at 477 nm). The next step follows the

421 "onion-peeling" approach proposed by Ortega et al. 2015 (the strong dependence of

422 scattering with wavelength means that shorter wavelengths result in shorter light

423 paths). We assign the UV (i.e. 360.8 nm) mixing ratios (mr_{uv}) and their expected

424 horizontal paths (d_{uv}) to the first peel (mr_A, meaning zone A). Then the second peel

425 (zone B, mr_B) can be derived as:

426

427 $$mr_B = \frac{mr_{vis} \times d_{vis} - mr_{uv} \times d_{uv}}{d_{vis}} \qquad (3)$$

428

429   Thereby, deriving mixing ratios (mr_a and mr_b) representative of two different

430 horizontal distances for each VAA.

431

432 **5 Results**

433

434 **5.1 O_4 and NO_2 DSCDs assessment**

435

436 An estimation of the overall goodness of the profile retrieval comes from the

437 correlation between the measured and simulated DSCDs for the entire campaign (Fig.

438 6). The fit between the measured and the simulated DSCDs shows correlations (r^2) very

439 close to 1 for both O_4 and NO_2 in the UV and VIS regions.

440

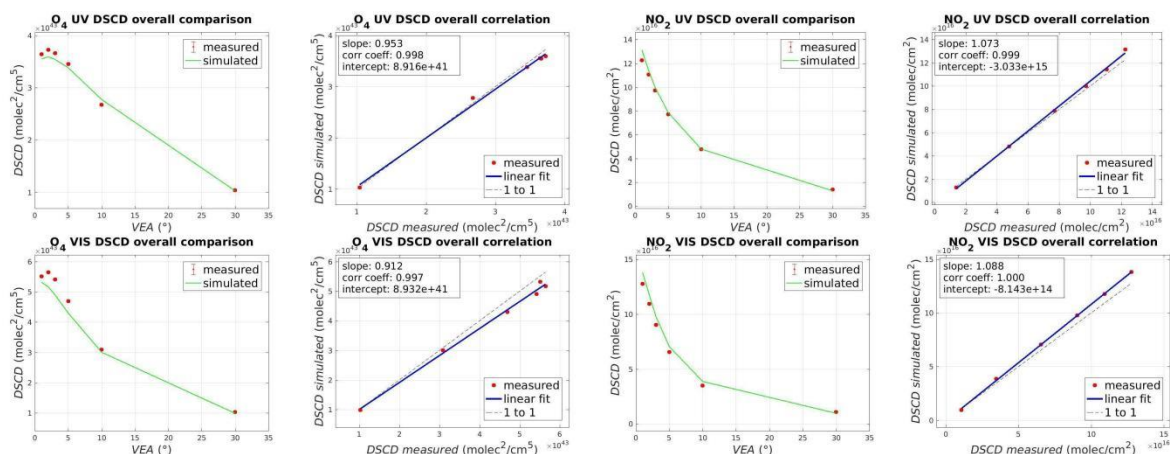**Figure 6**. Comparison between simulated and measured DSCDs of O_4 and NO_2. Red dots represent the measured DSCDs for each VEA, averaged over the entire campaign.

5.2 Two-dimensional maps

We now combine the VAA and height for each azimuthal cycle of the MAXDOAS-2D to generate a two-dimensional concentration map. Fig. 7 shows an example of the O_4 retrieval in the UV for a given azimuthal cycle. Fig. 7 also shows the comparison and correlation of measured and simulated DSCDs for that azimuthal cycle, along with the evolution of retrieved AOD. The AOD varies between 0.05 and 0.18 within this azimuthal cycle (Fig. 7, upper panel). The contour plot shows the irradiance extinction coefficient profiles with maximum values of 0.14 km^{-1} (near the ground and at around 40º VAA) associated with aerosol extinction (see discussion in Sect. 4.2). Note the enhanced extinction at about 2 km height pointing at 50 VAA. This could be due to uplift of particulate matter emitted by traffic (there is a main road at that location) (Carnerero et al., 2018). Further research is needed to better establish the vertical distribution of aerosols in Madrid, and their diurnal evolution.
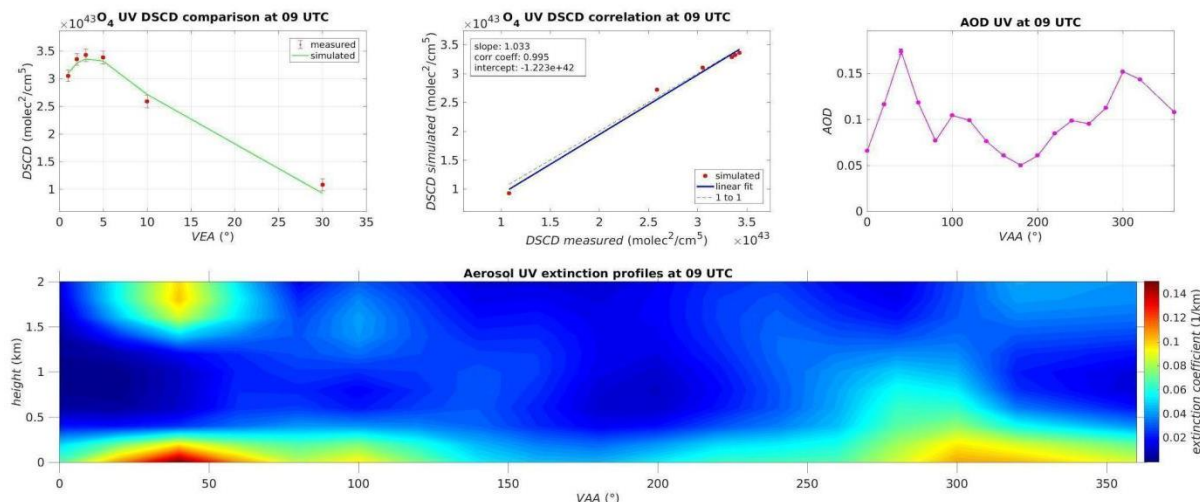
Figure 7. Example of O_4 and AOD retrievals in the UV region at 9 UTC on May 11, 2019. These contour plots are smoothed from adjacent VAA data points separated by 20º in order to estimate the azimuthal distribution of the irradiance extinction coefficients over Madrid.

Figure 8 shows a two-dimensional representation of NO_2 on May 11, 2019 at two different hours (6 UTC and 12 UTC, respectively). Both contour plots show maximum NO_2 values of 12 ppbv at 6 UTC and 8 ppbv at 12 UTC, when the instrument is pointing south (i.e. VAA of 180º). We chose to show this day as an example since it was a clear sky day and yielded NO_2 mixing ratios that were representative of the period of measurements. These values correspond to the layer near the ground and are in good agreement with our previous MAXDOAS observations in Madrid (Garcia-Nieto et al., 2018). The retrieved azimuthal distribution of NO_2 agrees with previous reports that show higher pollution levels in the southern part of Madrid (Picornell et al., 2019). NO_2 VCDs range from $5x10^{15}$ molecules cm^{-2} (at 12 UTC and pointing at 300° VAA) up to $15x10^{15}$ molecules cm^{-2} (at 12 UTC and pointing at 200º VAA), with an average value of $1x10^{16}$ molecules cm^{-2}. Although there are different NO_X emission rates at both times of the day (6 and 12 UTC), the increase in the boundary layer height

479 (de la Paz et al., 2016) during the day contribute to the similar values of VCDs at both

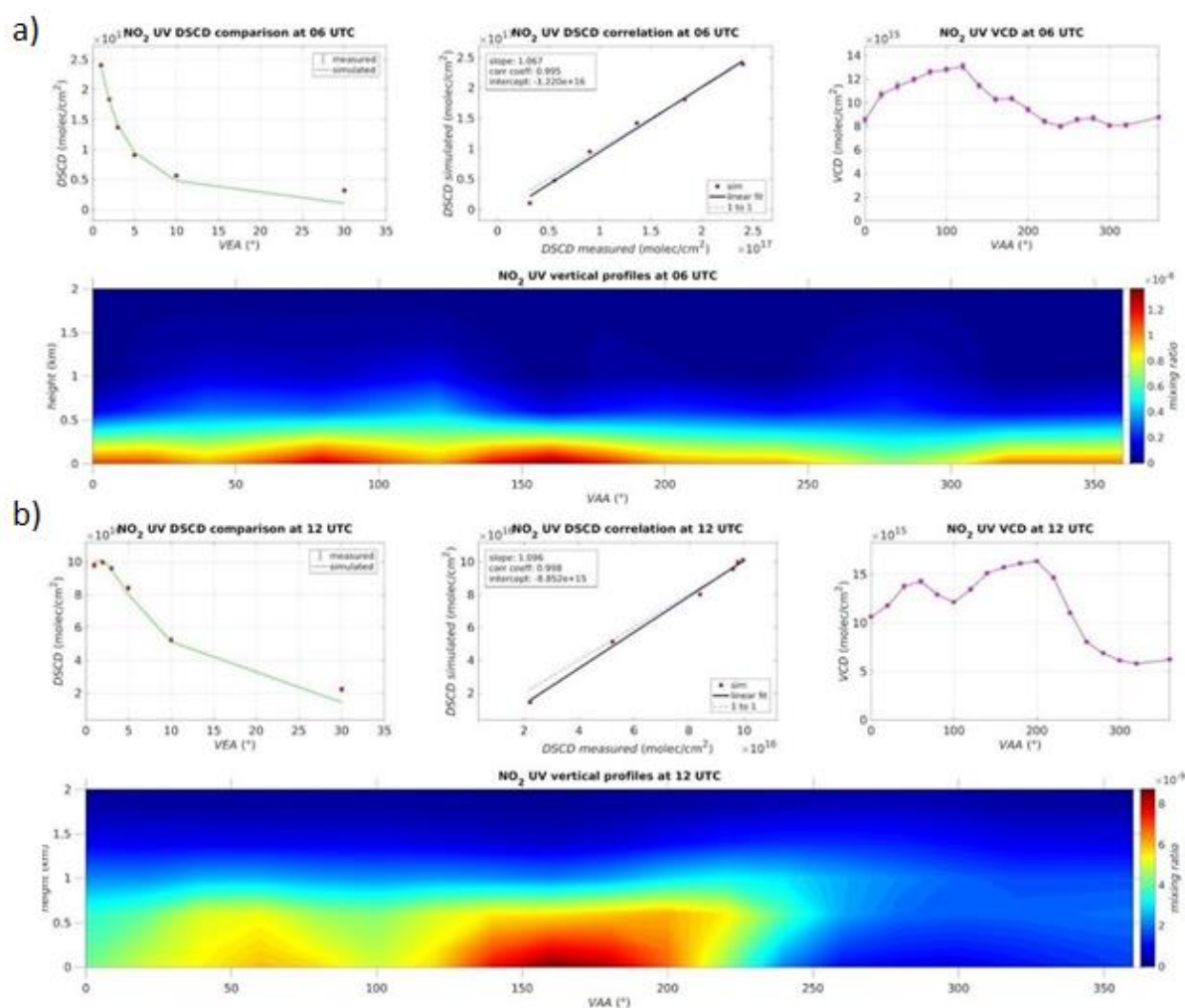480 hours but generally lower surface mixing ratios at 12 UTC.

481

482

Figure 8. NO₂ vertical distribution retrieved in the UV region at 6 UTC (a) and at 12 UTC
(b) on May 11, 2019. These contour plots are smoothed from adjacent VAA data points
separated by 20º in order to estimate the azimuthal distribution of NO₂ over Madrid.

486

487 We have also analyzed HONO DSCDs using the same DOAS analysis
488 configuration as in Garcia-Nieto et. al., 2018. Figure 9 shows a two-dimensional
489 representation of HONO on May 11, 2019 at 6 UTC. We retrieve surface layer peak
490 values of 0.7 ppbv pointing at 50° of VAA in the early morning, in agreement with

previous studies for HONO in urban environments (see Hendrick et al., 2014; Ryan et al., 2018). The VCDs at 6 UTC range from 6×10^{14} to 1.2×10^{15} molecule cm^{-2}.
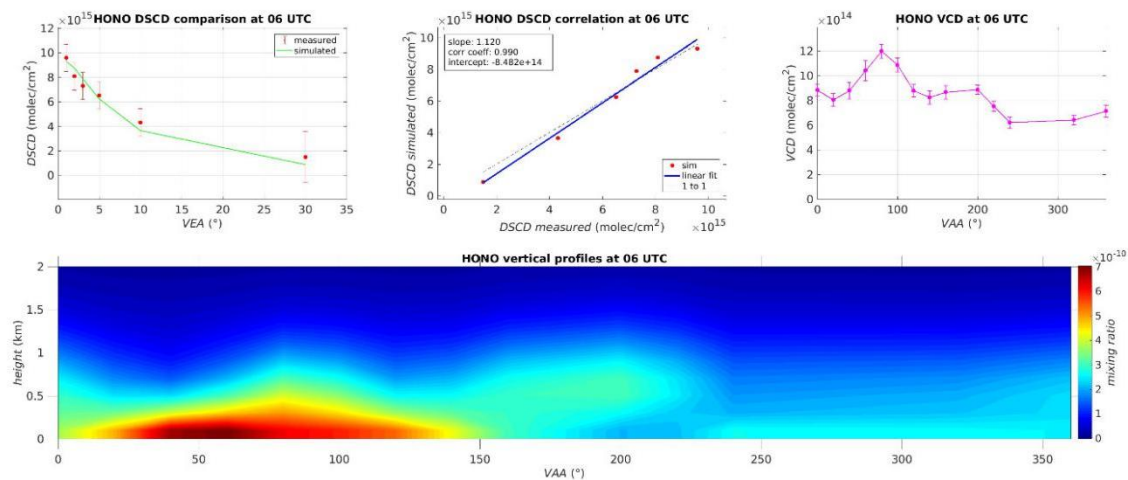

Figure 9. HONO vertical distribution retrieved in the UV region at 6 UTC. These contour plots are smoothed from adjacent VAA data points separated by 20° in order to estimate the azimuthal distribution of HONO over Madrid.

5.3 Horizontal distribution of NO₂

Based on Eq. (3), we derive the horizontal distribution of NO_2 in the surface layer (0-200 m height) using the measured NO_2 DSCDs at a VEA of 1° (which can safely be regarded as almost horizontal viewing, since its mean scattering height typically falls below 200 m height, i.e. within our ground layer). Figure 10 shows an example of surface layer NO_2 mixing ratios over two radial distances horizontally measured from the MAXDOAS-2D instrument (using the UV and the VIS NO_2, respectively, as explained in Section 4.3), located at the center of the plot. The highest mixing ratios occur during the first sunlit hours (7-8 UTC), coincident with the morning peak of NO_X emissions in Madrid (Quassdorff et al., 2016). This early morning peak is followed by a gradual decrease in surface layer NO_2 mixing ratios during the day. Note that NO_2 is

511 predominantly located in the southern part of the semisphere (VAA from 90º to 270º).

512 In follow up work we will combine the horizontal distribution of NO_2 with a chemical

513 transport model to further understand NO_2 transport dynamics throughout the day.
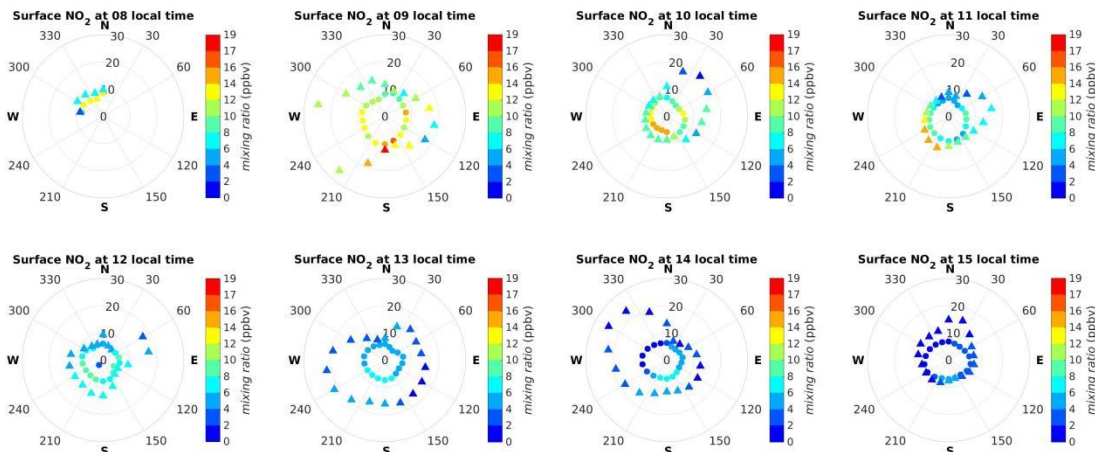
514

515

516 **Figure 10.** Polar plots of NO_2 within the surface layer (0-200 m height) for May 11,

517 2019. Please note that these polar plots extend over a direction perpendicular to those

518 shown in Fig. 8. Here, circles are used for the UV (shorter horizontal light path) and

519 triangles for the VIS (larger horizontal light path). Both symbols stand for the mean

520 horizontal light path within the surface layer at each spectral region.

521

522 **5.4 Correlation with Madrid´s in-situ air quality monitoring stations**

523

524   We suggest that MAXDOAS-2D mesoscale observations may complement the

525 information provided by the local air quality monitoring network based on reference

526 analytical techniques (according to Directive 2008/50/EC). While air quality monitors

527 of the reference network provide information about ambient concentrations in their

528 specific locations (currently 24 air quality monitoring stations measure NO_2 within the

529 city, see AM, 2019), MAXDOAS-2D observations produce near ground-level

530 concentrations averaged over the optical path in a given direction. That prevents us

531 from quantitatively comparing both types of observations. Nonetheless, we analyzed

532 their correspondence using the NO_2 concentrations measured by the in-situ

533 instruments throughout the entire city, and the NO_2 mixing ratios within the surface

534 layer derived from our MAXDOAS-2D instrument over the 2-month period (May-June,

535 2019). For this comparison, we considered the air quality monitoring stations within a

536 distance from the MAXDOAS-2D equal or lower than 10 km (thus remaining 20 air

537 quality monitoring stations). Since this is the typical horizontal light path for the UV

538 region, we decided to include only the NO_2 values retrieved in the UV region for the

539 comparison. Strong gradients between the values measured by the in-situ instruments

540 are typical. Therefore, and considering that we are mainly interested in their temporal

541 correlation with respect to our measurements, we compare both the in-situ NO_2 and

542 surface layer MAXDOAS-2D hourly-averaged data. Note that for the MAXDOAS-2D,

543 this approximately corresponds to averaging the surface layer values for each

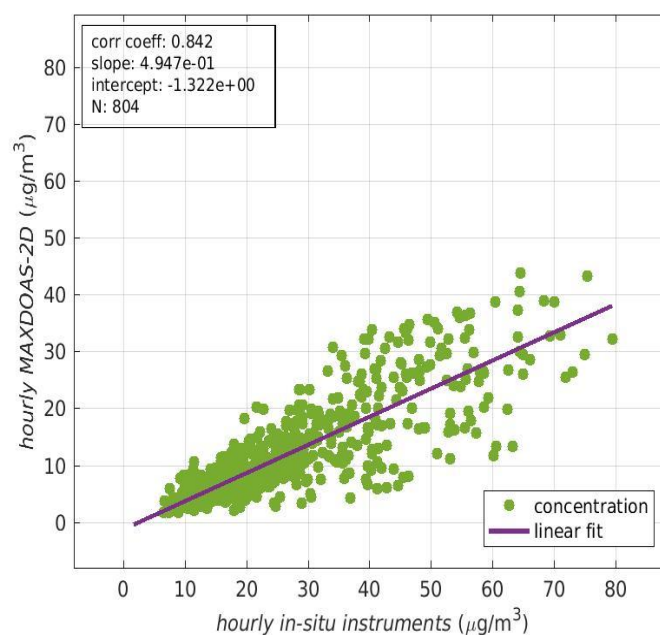544 azimuthal lap, given that each azimuthal lap takes approximately 1 hour to complete.

545

546

547 **Figure 11**. Correlation between in-situ observations from Madrid´s air quality

548   monitoring network and those derived from the MAXDOAS-2D instrument for the

549   surface layer (0-200 m height).

550

551   Despite the different spatial representativeness, Figure 11 shows a reasonably

552   good correlation coefficient of 0.842 between both datasets for the two-month

553   campaign. The slope is lower than 1, this can be explained by the typical NO_2 vertical

554   profiles in urban environments. Simulations performed over Madrid with a high-

555   resolution Eulerian air quality model (Borge et al., 2018) yielded an exponentially

556   decreasing with height NO_2 profile. Therefore, the MAXDOAS-2D mixing ratios, which

557   represent an average across the surface layer (0-200 m height), are not expected to

558   quantitatively match the values of in-situ instruments, located close to the surface

559   (between 0-10 m height). Similar conclusions -and slopes comparable to the one

560   retrieved above- regarding the correlation between in-situ and MAXDOAS instruments

561   can be found in previous works (Schreier et al., 2020; Kramer et al., 2008; Chan et al.,

562   2020). In addition, there is a good temporal correlation between in-situ and

563   MAXDOAS-2D measurements over an extended period of time.

564

565   **6 Summary and Conclusions**

566

567   An analysis of O_4, NO_2 and HONO vertical concentration profiles in the urban

568   atmosphere of Madrid (Spain) has been performed over two months (from May 6 to

569   July 5, 2019). We analyzed the absorptions and derived the corresponding DSCDs for

570   both trace gases in the UV and VIS regions. Then, the corresponding profiles were

571   retrieved using a RTM. In this step, we assessed the impact of different atmospheric

572   profiles (pressure and temperature) in the retrieval results, and found that the set of

573   chosen atmospheric profiles has a small impact on the O_4 retrieval and the estimation

574   of light paths. However, there is a noticeable change in the irradiance extinction

575 profiles, which makes difficult to quantitatively assign extinction due to aerosols,
576 especially in heights above the boundary layer.

577 The overall comparison of measured and simulated trace gas DSCDs showed
578 that they were in very good agreement (with correlation coefficients close to 1),
579 supporting the reliability of the observations. The MAXDOAS-2D instrument provides
580 the first two-dimensional view (in height and VAA) of pollution concentration in the
581 city of Madrid. Exploring one day (May 11, 2019) we compared two hours: the peak
582 rush hour and noon time, obtaining NO_2 maximum values of 12 ppbv and 8 ppbv
583 respectively, both maxima pointing to the south direction. Two-dimensional HONO
584 measurements were also made with mixing ratio peaks of 0.7 ppbv in the early
585 morning, and VCDs ranging from $6x10^{14}$ to $1.2x10^{15}$ molecule cm^{-2}.

586

587 We have also inferred information on the horizontal gradient of NO_2 within the
588 surface layer making use of the strong dependence between wavelengths and light
589 paths across the NO_2 absorption spectrum. The resulting "onion-peeling" figures
590 indicate peak values of NO_2 in the early morning and in the southern section of the city
591 (around 180 º VAA), it resulted in a gradual decrease in NO_2 mixing ratios during the
592 day, maximum values of NO_2 appear in the southern part of the semisphere. Finally,
593 we suggest that the new mesoscale information provided by the MAXDOAS-2D
594 instrument helps in the study of pollution transport dynamics. MAXDOAS-2D and in-
595 situ instruments provide different information, and thus, combining both can improve
596 our understanding of the complex issue of air pollution in the city of Madrid.

597

598 **Author Contribution**

599

600   A.S-L. devised the research. D.G-N. and N.B. carried out the measurements and

601   analyzed the data. D.G-N., N.B., R.G. and A.S-L. analyzed and interpreted the results.

602   D.G-N. wrote the manuscript with contributions from all co-authors.

603

604   **Acknowledgements**

605

614

615   **References**

616

617   Ayuntamiento de Madrid (AM): Madrid 2016 Annual Air Quality Assessment Report

618   (Calidad del aire Madrid 2019). General Directorate of Sustainability and

619   Environmental Control, Madrid City Council   Available online -only Spanish version-

620   at

621   http://www.mambiente.munimadrid.es/opencms/export/sites/default/calaire/Anex

622   os/Memorias/Memoria_2019.pdf, 2019.

623

624 Benavent, N., Garcia-Nieto, D., Wang, S., & Saiz-Lopez, A.: MAX-DOAS measurements
625 and vertical profiles of glyoxal and formaldehyde in Madrid, Spain. Atmospheric
626 Environment, 199, 357–367, 2019.

627

628 Borge, R., Narros, A., Artínano, B., Yagüe, C., et al.: Assessment of micro- scale spatio-
629 temporal variation of air pollution at an urban hotspot in Madrid (Spain) through an
630 extensive field campaign. Atmos. Environ. 140, 432–445, 2016.

631

632 Borge, R., Santiago, J. L., de la Paz, D., Martín, F., Domingo, J., Valdés, C., Sánchez, B.,
633 Rivas, E., Rozas, M. T., Lázaro, S., Pérez, J., & Fernández, Á.: Application of a short term
634 air quality action plan in Madrid (Spain) under a high-pollution episode - Part II:
635 Assessment from multi-scale modelling. Science of the Total Environment, 635, 1574–
636 1584. https://doi.org/10.1016/j.scitotenv.2018.04.323, 2018.

637

638 Carnerero, C., Pérez, N., Reche, C., Ealo, M., Titos, G., Lee, H.-K., Eun, H.-R., Park, Y.-H.,
639 Dada, L., Paasonen, P., Kerminen, V.-M., Mantilla, E., Escudero, M., Gómez-Moreno, F.
640 J., Alonso-Blanco, E., Coz, E., Saiz-Lopez, A., Temime-Roussel, B., Marchand, N.,
641 Beddows, D. C. S., Harrison, R. M., Petäjä, T., Kulmala, M., Ahn, K.-H., Alastuey, A., and
642 Querol, X.: Vertical and horizontal distribution of regional new particle formation
643 events in Madrid, Atmos. Chem. Phys., 18, 16601–16618,
644 https://doi.org/10.5194/acp-18-16601-2018, 2018.

645

646 Chan, K. L., Wiegner, M., Alberti, C., & Wenig, M.: MAX-DOAS measurements of
647 tropospheric NO_2 and HCHO in Munich and the comparison to OMI and TROPOMI
648 satellite observations. Atmospheric Measurement Techniques Discussions, 2020.

649

650 Chance, K., Kurucz, R.L.: An improved high-resolution solar reference spectrum for
651 earth's atmosphere measurements in the ultraviolet, visible, and near infrared. J.
652 Quant. Spectrosc. Radiat. Transf.; Special Issue Dedicated to Laurence S. Rothman on
653 the Occasion of his 70th Birthday 111 (9), 1289-1295, 2010.

654

655 Clémer, K., Van Roozendael, M., Fayt, C., Hendrick, F., Hermans, C., Pinardi, G., Spurr,
656 R.,Wang, P., De Mazière, M.: Multiple wavelength retrieval of tropospheric aerosol
657 optical properties from MAXDOAS measurements in Beijing. Atmospheric
658 Measurement Techniques 3 (4), 863, 2010.

659

660 Cuevas, C., Notario, A., Adame, J. Hilboll, A., Richter, A., Burrows, J.P, Saiz-Lopez, A.:
661 Evolution of NO2 levels in Spain from 1996 to 2012. Sci Rep 4, 5887, 2014.

662

663 de la Paz, D., Borge, R., & Martilli, A.: Assessment of a high resolution annual WRF-
664 BEP/CMAQ simulation for the urban area of Madrid (Spain). Atmospheric
665 Environment, 144, 282–296. https://doi.org/10.1016/j.atmosenv.2016.08.082, 2016.

666

667 Dimitropoulou, E., Hendrick, F., Pinardi, G., Friedrich, M., Merlaud, A., Tack, F., De
668 Longueville, H., Fayt, C., Hermans, C., Laffineur, Q., Fierens, F., & Van Roozendael, M.:
669 Validation of TROPOMI tropospheric NO_2 columns using dual-scan MAX-DOAS
670 measurements in Uccle, Brussels. Atmospheric Measurement Techniques Discussions,
671 2020.

672

673 European Environment Agency (EEA).: Air quality in Europe – 2019 report. EEA
674 Technical Report No 10/2019. ISBN: 978-92-9480-088-6. Available online at:
675 http://www.eea.europa.eu/publications/air-quality-in-europe-2019., 2019

676

677   Hendrick, F., Müller, J.-., Clémer, K.,Wang, P., De Mazière,M., Fayt, C., Gielen, C.,

678   Hermans, C., Ma, J., Pinardi, G., Stavrakou, T., Vlemmix, T., Van Roozendael, M.: Four

679   years of ground-based MAX-DOAS observations of HONO and NO_2 in the Beijing area.

680   Atmos. Chemical Physics, 14 (2), 765, 2014.

681

682   Garcia-Nieto, D., Benavent, N., Saiz-Lopez, A.: Measurements of atmospheric HONO

683   vertical distribution and temporal evolution in Madrid (Spain) using the MAXDOAS

684   technique. Science of the Total Environment. 643, 957–966, 2018.

685

686   Hönninger, G., von Friedeburg, C., Platt, U.: Multi axis differential optical absorption

687   spectroscopy (MAXDOAS). Atmos. Chem. Phys. 4 (1), 231-254, 2004.

688

689   Izquierdo, R., García Dos Santos, S., Borge, R., Paz, D. de la, Sarigiannis, D., Gotti, A., &

690   Boldo, E.: Health impact assessment by the implementation of Madrid City air-quality

691   plan in 2020. Environmental Research, 183, 109021, 2020.

692

693   Kramer, L. J., Leigh, R. J., Remedios, J. J., & Monks, P. S: Comparison of OMI and ground-

694   based in situ and MAX-DOAS measurements of tropospheric nitrogen dioxide in an

695   urban area. Journal of Geophysical Research Atmospheres, 2008.

696

697   Meller, R., Moortgat, G.K.: Temperature dependence of the absorption cross sections

698   of formaldehyde between 223 and 323 K in the wavelength range 225-375 nm. Journal

699   of Geophysical Research: Atmosphere 105, 7089-7101, 2000.

700

Monks, P. S., Granier, C., Fuzzi, S., Stohl, A., Williams, M. L., Akimoto, H., Amann, M.,Baklanov, A., Baltensperger, U., Bey, I., Blake, N., Blake, R. S., Carslaw, K., Cooper, O. R., Dentener, F., Fowler, D., Fragkou, E., Frost, G. J., Generoso, S., … von Glasow, R.: Atmospheric composition change - global and regional air quality. Atmospheric Environment, 43(33), 5268–5350. https://doi.org/10.1016/j.atmosenv.2009.08.021, 2009.

Ortega, I., Koenig, T., Sinreich, R., Thomson, D., Volkamer, R.: The CU 2-D-MAX-DOAS instrument – Part 1: Retrieval of 3-D distributions of NO2 and azimuth-dependent OVOC ratios. Atmospheric Measurement Technique, 8, 2371-2395, 2015.

Peters, E., Wittrock, F., GroBmann, K., FrieB, U., Richter, A., Burrows, J.: Formaldehyde and nitrogen dioxide over the remote western Pacific Ocean: SCIAMACHY and GOME-2 validation using ship-based MAX-DOAS observations. Atmospheric Chemistry and Physics. 12 (22), 11179, 2012.

Picornell, M., Ruiz, T., Borge, R. et al. Population dynamics based on mobile phone data to improve air pollution exposure assessments. J Expo Sci Environ Epidemiol 29, 278–291. https://doi.org/10.1038/s41370-018-0058-5, 2019.

Plane, J.M.C., Saiz-Lopez, A.: UV-Visible Differential Optical Absorption Spectroscopy (DOAS). In: Heard, D.E. (Ed.), Analytical Techniques for Atmospheric Measurement. Blackwell Publishing, Oxford, 2006.

Platt, U., Stutz, J.: Differential Optical Absorption Spectroscopy: Principles and Applications. Springer Berlin Heidelberg, Berlin, Heidelberg, Berling, Heidelberg, 2008.

727

728   Quaassdorff C, Borge R, Pérez J, Lumbreras J, de la Paz D, de Andrés JM. Microscale

729   traffic simulation and emission estimation in a heavily trafficked roundabout in Madrid

730   (Spain). Sci Total Environ, 566-567:416-427. doi:10.1016/j.scitotenv.2016.05.051,

731   2016.

732

733   Rodgers, C.D.: Inverse Methods for Atmospheric Sounding: Theory and Practice. World

734   Scientific Publishing, Singapore (Singapore), 2000.

735

736   Rothman, L.S., Gordon, I.E., Barber, R.J., Dothe, H., Gamache, R.R., Goldman, A.,

737   Perevalov, V.L., Tashkum, S.A., Tennyson, J.: HITEMP, the high-temperature molecular

738   spectroscopic database Journal of Quantitative Spectroscopy and Radiative Transfer.

739   111 (15), 2139, 2150, 2010.

740

741   Ryan, R. G., Rhodes, S., Tully, M., Wilson, S., Jones, N., Frieß, U., and Schofield, R.:

742   Daytime HONO, NO_2 and aerosol distributions from MAX-DOAS observations in

743   Melbourne, Atmos. Chem. Phys., 18, 13969–13985, 2018.

744

745   Saiz-Lopez, A., Borge, R., Notario, A. et al.: Unexpected increase in the oxidation

746   capacity of the urban atmosphere of Madrid, Spain. Sci Rep 7, 45956.

747   https://doi.org/10.1038/srep45956, 2017.

748

749   Schreier, S. F., Richter, A., Peters, E., Ostendorf, M., Schmalwieser, A. W., Weihs, P., &

750   Burrows, J. P: Dual ground-based MAX-DOAS observations in Vienna, Austria:

751 Evaluation of horizontal and temporal NO2, HCHO, and CHOCHO distributions and

752 comparison with independent data sets. Atmospheric Environment: X 5, 2020

753

754 Serdyunchenko, A., Gorshelev, V., Weber, M., Chehade, W., Burrows, J.P.: High

755 spectral resolution ozone absorption cross-sections – Part 2: temperature

756 dependence. Atmospheric Measurement Techniques. 7 (2), 625-636, 2014.

757

758 Solomon, S., & Sanders, Ryan W and Schmeltekopf, A. L.: On the Interpretation of

759 Zenith Sky Absorption Measurements. Journal of Geophysical Research, 92, 8311–

760 8319, 1987.

761

762 Stutz, J., Kim, E.S., Platt, U., Bruno, P., Perrino, C., Febo, A.: UV-visible absorption cross

763 sections of nitrous acid. Journal of Geophysical Research: Atmosphere. 105, 14585-

764 14592, 2000.

765

766 Thalman, R., Volkamer, R.: Temperature dependent absorption cross-sections of O2-

767 O2 collision pairs between 340 and 630 nm and at atmospherically relevant pressure.

768 Physical Chemistry Chemical Physics 15 (37), 15371-15381, 2013.

769

770 Vandaele, A.C., Hermans, C., Simon, P.C., Carleer, M., Colin, R., Fally, S., Mérienne,

771 M.F., Jenouvrier, A., Coquart, B.: Measurements of the NO2 absorption cross-section

772 from 42000 cm^-1 to 10000 cm^-2 (238-1000 nm) at 220 K and 294 K. Journal of

773 Quantitative Spectroscopy and Radiative Transfer; Atmospheric Spectroscopy

774 Application 59 (3), 171-184 96, 1998.

775

776 Volkamer, R., Spietz, P., Burrows, J., Platt, U.: High-resolution absorption cross-section

777 of glyoxal in the UV-vis and IR spectral ranges. J. Photochem. Photobiol. Chem. 172 (1),

778 35-46, 2005.

779

780 Wagner, T., Beirle, S., Benavent, N., Bösch, T., Chan, K. L., Donner, S., Dörner, S., Fayt,

781 C., Frieß, U., García-Nieto, D., Gielen, C., González-Bartolome, D., Gomez, L., Hendrick,

782 F., Henzing, B., Jin, J. L., Lampel, J., Ma, J., Mies, K., Navarro, M., Peters, E., Pinardi, G.,

783 Puentedura, O., Puķīte, J., Remmers, J., Richter, A., Saiz-Lopez, A., Shaiganfar, R.,

784 Sihler, H., Van Roozendael, M., Wang, Y., and Yela, M.: Is a scaling factor required to

785 obtain closure between measured and modelled atmospheric O4 absorptions? An

786 assessment of uncertainties of measurements and radiative transfer simulations for 2

787 selected days during the MAD-CAT campaign. Atmospheric Measurement Techniques

788 12, 2745–2817, 2019.

789

790 Wang, S., Cuevas, C.A., Frieß, U., Saiz-Lopez, A.: MAX-DOAS retrieval of aerosol

791 extinction properties in Madrid, Spain. Atmospheric Measurement Techniques

792 9,5089–5101, 2016.

793

794 World Health Statistics (WHO): monitoring health for the SDGs. Wold Health

795 Organization, 2019.

796

797 Yang, T., Si, F., Luo, Y., Zhan, K., Wang, P., Zhou, H., Zhao, M., & Liu, W.:Source

798 contribution analysis of tropospheric NO_2 based on two-dimensional MAX-DOAS

799 measurements. Atmospheric Environment, 2019.